Femtosecond realtime probing of reactions. III. Inversion to the potential from femtosecond transitionstate spectroscopy experiments

Richard B. Bernstein and Ahmed H. Zewail

Articles you may be interested in

Femtosecond realtime probing of reactions. XXI. Direct observation of transitionstate dynamics and structure in chargetransfer reactions
J. Chem. Phys. **105**, 6216 (1996); 10.1063/1.472478

Femtosecond realtime probing of reactions. IV. The reactions of alkali halides
J. Chem. Phys. **91**, 7415 (1989); 10.1063/1.457266

Femtosecond realtime probing of reactions. II. The dissociation reaction of ICN
J. Chem. Phys. **89**, 6128 (1988); 10.1063/1.455428

Femtosecond realtime probing of reactions. I. The technique
J. Chem. Phys. **89**, 6113 (1988); 10.1063/1.455427

Realtime femtosecond probing of "transition states" in chemical reactions
J. Chem. Phys. **87**, 2395 (1987); 10.1063/1.453122

Femtosecond real-time probing of reactions. III. Inversion to the potential from femtosecond transition-state spectroscopy experiments

Richard B. Bernstein
Department of Chemistry and Biochemistry, University of California, Los Angeles, California 90024-1569

Ahmed H. Zewail[a)]
Arthur Amos Noyes Laboratory of Chemical Physics,[b)] California Institute of Technology, Pasadena, California 91125

Femtosecond transition-state spectroscopy (FTS) of elementary reactions [M. Dantus, M. J. Rosker, and A. H. Zewail, J. Chem. Phys. **87**, 2395 (1987)] provides real-time observations of photofragments in the process of formation. A classical mechanical description of the time-dependent absorption of fragments during photodissociation [R. Bersohn and A. H. Zewail, Ber. Bunsenges. Phys. Chem. **92**, 373 (1988)] forms the basis for the present scheme for relating observations to the potential energy surface. A direct inversion scheme is presented that allows the difference in the two relevant excited-state potential curves to be deduced from observed transients at different probe wavelength tunings. In addition, from the shape and dependence of the transients on pump wavelength, information on the lower of the two potential curves (i.e., that of the dissociating molecule) is obtained. The methodology is applied to the experimental FTS data (Dantus *et al.*) on the CN photofragment from the ICN photodissociation.

I. INTRODUCTION

Femtosecond transition-state spectroscopy (FTS) has been reported for several elementary reactions involving direct dissociation or trapping (resonances) of photofragments en route to dissociation.[1-3] The general concept of the experiment is simple: a pump femtosecond pulse at λ_1 excites a target molecule, say ABC, at $t = 0$, to a repulsive electronic state and the probe femtosecond pulse at λ_2, delayed by a variable time t, detects the photofragment (product), say BC, as it is being formed, in the process of separation from A. The probe laser is first tuned to a wavelength λ_2^{∞} corresponding to a known excitation resonance of the stable BC (i.e., at essentially infinite separation from A) species inducing either fluorescence (LIF)[1-3] or multiphoton ionization time of flight (MPI-TOF),[4] allowing its detection. The resulting photon or photoion signal is recorded as one point on a curve of $I(t)$. The delay is altered systematically until an entire curve of $I(t)$ at $\lambda = \lambda_2^{\infty}$ is obtained. The $I(t)$ curve shows an induction period indicative of the time required for the BC species to separate effectively from the force field of A and attain asymptotically its "normal" identity as BC in its final state. At this point of separation, the fragment achieves its asymptotic recoil velocity governed by E'_{tr}, the final translational energy, which, in turn, is determined by the total available energy E_{avl} minus the internal energy of the products.

The wavelength of the laser is detuned by a small increment Δ_{λ} to the red (or the blue) of this value of λ_2^{∞} to a new value λ_2^{*} and the $I(t;\Delta_{\lambda})$ curve is recorded. This curve goes through a maximum at short delays and then decays to asymptotically constant intensities, dependent upon the particular chosen value of the detuning increment Δ_{λ}. When a series of such experiments is carried out at selected values of Δ_{λ}, the resulting body of data constitute a surface, $I(t,\Delta_{\lambda};\lambda_1,\lambda_2)$. Such a data base contains a great deal of information on the potential energy surface (or its 2D projection, the relevant potential curve) for the formation of BC from the excited state ABC, which leads to the detected BC photofragment.

Before going into a detailed theoretical discussion, we consider the gross features of the experimental observations,[1-3] taking the ICN reaction as an example:

$$\text{ICN}^* \rightarrow [\text{I}\cdots\text{CN}]^{\ddagger *} \rightarrow \text{I} + \text{CN}(v,j) + E'_{\text{tr}}.$$
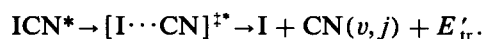
Shown in Fig. 1 is the on-resonance ($\Delta_{\lambda} = 0$) curve, $I(t;\lambda_2^{\infty})$. There is a 205 fs delay[2(b)] before the CN has "escaped" from the I atom and its energy levels become those of the isolated CN molecule, so it can absorb the λ_2^{∞} photon at 388.5 nm. For curve (b), $I(t;\lambda_2^{*})$ where $\lambda_2^{*} = \lambda_2^{\infty} + \Delta_{\lambda}$, the signal rises at an earlier time at the separation $R = R^*$ [corresponding to λ_2^{*} in Fig. 1(a)]. At R^*, the wavelength λ_2^{*} is just correct for the excitation of the CN fragment from V_1 to V_2 [as seen in Fig. 1(a)], i.e., the photon energy $\text{hc}/\lambda_2^{*} = V_2(R^*) - V_1(R^*)$. The signal falls to a finite value because the bandwidth of the laser pulse is finite and so the free CN has some residual absorption (i.e., absorption of the blue wing of the probe laser pulse). This spectral bandwidth is actually the "window" onto the potential for fragment separation. Typically, for pulses of 40 to 200 fs, the corresponding transform-limited widths are 330 to 66 cm^{-1}, respectively.

Bersohn and Zewail have presented a classical mechanical theory[5] for the time-dependent absorption of the fragments in the course of the reaction. Assuming the usual quasidiatomic model and simple analytical functional forms for the relevant excited-state potential curves $V_1(R)$ and $V_2(R)$, and taking the laser wavelength profile to be Lorent-
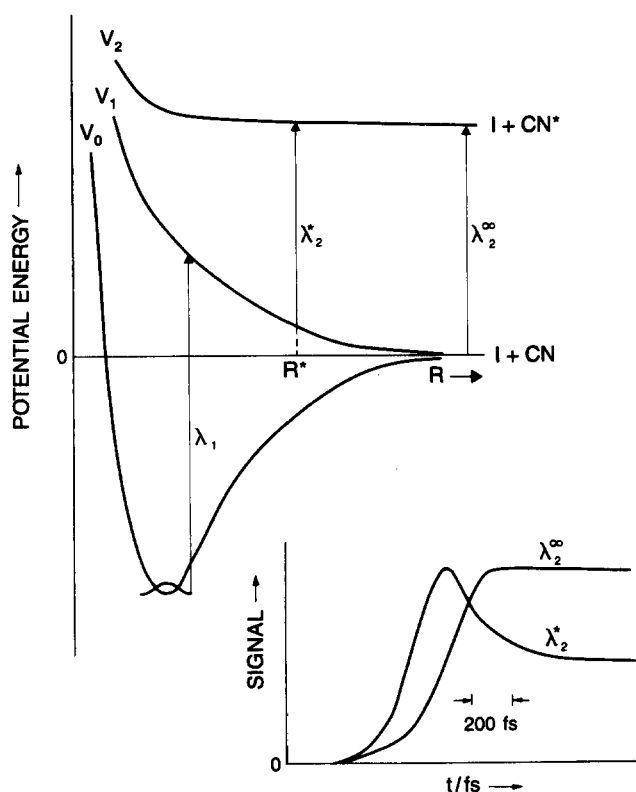

FIG. 1. Schematic diagram (see Ref. 2) showing the relevant pseudodiatomic potentials for ICN that explicate the experimental FTS data of Ref. 2. The pump-laser wavelength is λ_1 and the probe-laser wavelength is λ_2. When the probe-laser wavelength is set at λ_2^∞, it detects free CN, but when red detuned to λ_2^*, it detects the transition states $[I \cdots CN]^{\ddagger*}$ at separation R^*. The inset shows smoothed experimental transients from Ref. 2(a), one on-resonance probe at $\lambda_2^* = 388.59$ nm ($\Delta = 0$), one detuned by $\Delta = 40$ cm^{-1} to the red. The pump-laser wavelength was ~ 306 nm.

zian, they derived explicit equations for the functions $I(t,\lambda)$ in terms of the assumed potential parameters and the Lorentzian half-width γ.

For the simplest case in which $V_1(R)$ is a pure exponential repulsion, $V_1(R) = V_1 \exp(-R/L_1)$ and assuming that the upper potential is flat, i.e., $V_2(R) = V_2$ (at least for $R > R^*$), they obtained a simple result for $I(t,\lambda)$ that can be expressed analytically in the form

$$I(t,t^*) = \eta[\gamma^2 + E^2(\text{sech}^2 x - \text{sech}^2 x^*)^2]^{-1}, \quad (1)$$

where η is a constant carrying units of intensity. Here $E \equiv E_{tr}' = \tfrac{1}{2}\mu v^2$ is the terminal value of the relative translational energy, v the final relative velocity of the fragments (of reduced mass μ), while $x \equiv vt/2L_1$ and $x^* \equiv vt^*/2L_1$, with t^* defined as $t^* = t(R^*)$, the time corresponding to the separation R^*. The Lorentzian half-width γ has the same units as E (typically, wave numbers).

Applying this equation to the ICN data led to a value of the potential constant L_1. The general shape of the $I(t,\lambda)$ experiment curves was qualitatively reproduced by the functional form of Eq. (1), and it was found to be sensitive to the shape of the potential.

The goal of the present work is to provide a procedure for direct "inversion" of such experimental data on detuned transients in order to yield quantitative information on the

relevant excited-state potential surfaces *without* making assumptions about their functional form, or about the spectral line shape of the probe laser. In addition, it is of interest to ascertain the influence of the pump-laser photon energy upon the experimentally observable $I(t,\lambda)$ data and thus derive independent information on the lowest excited state of the ABC molecule.

II. THE INVERSION METHOD

What follows is a hierarchy of treatments of the "generic" transient detuning experiment, starting from the simplest model approach and then dealing with successively more realistic systems. Throughout, we limit our treatment to a classical mechanical description of the half-collision (i.e., the fragment recoil velocities). For most of what follows, we assume a diatomic or quasidiatomic system where the BC fragment is considered "structureless" and therefore noted as B. Thus, instead of ABC* → A + BC, we shall use AB* → A + B.

We require only a knowledge of the available energy $E_{avl} = E_{exc} - D_{AB}^0$, obtained from the laser excitation photon energy E_{exc} (and any initial energy in AB) and the bond dissociation energy of AB, and the excited-state potential energy curve $V_1(R)$. Energy conservation is expressed

$$E_{avl} = V_1[R(t)] + \tfrac{1}{2}\mu\left(\frac{dR}{dt}\right)^2, \quad (2)$$

so

$$\frac{dR}{dt} = (2/\mu)^{1/2}\{E_{avl} - V_1[R(t)]^{1/2}\}$$
$$= v\{1 - V_1[R(t)]/E_{avl}\}^{1/2}, \quad (3)$$

where the terminal velocity is $v = (2E_{avl}/\mu)^{1/2}$.

For many cases, the available energy is much larger than the potential energy $V_1(R^*)$ at the minimum separation $R^*(\equiv R_{min}^*)$ probed at t_{min}^* by the probe laser pulse, so Eq. (3) reduces to

$$\frac{dR}{dt} \simeq v \quad (\text{for} \quad t \geqslant t_{min}^*) \quad (4)$$

so that

$$R(t) = R_{min}^* + v(t - t_{min}^*), \quad (5)$$

i.e.,

$$R = vt + \text{const.}, \quad (6)$$

in the region of R probed. Thus, in this large-R domain, the shapes of $V(R)$ and $V(t)$ are identical, with only a scale change for the abscissa. In most of what follows, we will deal entirely with the time domain, seeking to evaluate $V_1(t)$ from the experimental observations.

A. Inversion from probe-laser wavelength detuning experiments

Here, we consider the detection process, in which the probe laser excites the separating-fragment system AB* to a higher excited state of AB, namely $V_2(R)$, where fluorescence allows detection in the LIF mode (or what is the "doorway state" in the MPI detection mode).
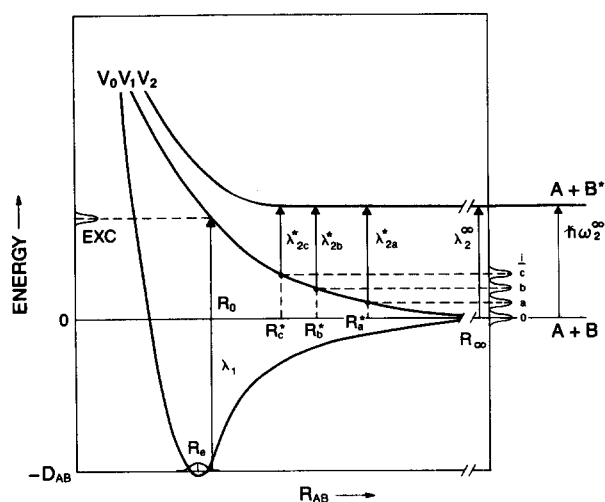
FIG. 2. Similar to Fig. 1, but more detailed schematic diagram, appropriate to a quasidiatomic molecule AB, showing the several "windows" to the potential V_1 for the probe laser detuned successively to the red by amounts Δ_i ($i = 0, a, b$, and c), corresponding to $R^* = \infty, R_a^*, R_b^*$, and R_c^*, as shown. Note that the upper potential, V_2, is assumed to be flat for $R > R_c^*$.

Case 1. Single repulsive surface

Figure 2 shows a set of potential curves appropriate for illustrations of the model at the most primitive level, with the lower excited state V_1 purely repulsive, and the upper one V_2 essentially flat in the region of the separations probed. Detuning by linearly increasing Δ_i ($i = 0, a, b, c$), as shown, probes R values from asymptotic ($R \rightarrow \infty$) to $R = R_a^*, R_b^*$, and R_c^*, respectively. For sufficiently sharp (temporal) probe pulses and *extremely* sharp pump laser pulses, assumed throughout, one would expect a sequence of $I(t,\Delta)$ curves in which each rises to a sharp peak at time $t_i(R_i^*) \equiv t_i^*$, all peaks of the same height, say I_{max}. For
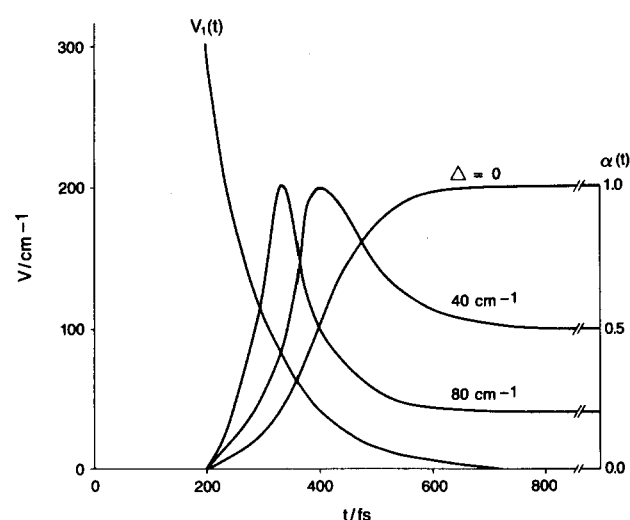
$\Delta = 0$, the intensity should rise monotonically to approach I_{max}. This behavior is illustrated in Fig. 3.

In the case where the spectral bandwidth of the fs probe laser is greater than the typical detuning increment Δ, the situation is different. The pulse probes a *range* of t values around t_i. The temporal response, i.e., $I(t;\Delta)$, will directly reflect the projection of the spectral bandwidth of the probe laser onto the potential; it will be the weighted sum (i.e., superposition) of the absorptions of an infinite set of delta functions (in frequency) whose envelope is the spectral profile of the probe laser.

Figure 4 displays the $I(t,\Delta)$ surface taken from the "raw data"[6] of Ref. 2, i.e., $I(t)$ for probe detunings (to the red of the wavelength for the free CN fragment) of zero, 40 and 106 cm^{-1}.[2] The asymptotic values of the normalized signal levels reflect the near-Lorentzian probe laser spectral line shape. Thus for $\Delta = 0$, the intensity rises after a delay time sufficient for the CN to have become essentially "free" of the I fragment, to its asymptotic final value, say, unity. For $\Delta = 40$ cm^{-1}, i.e., the nominal probe wavelength offset by 40 cm^{-1} to the red, the peak signal occurs earlier (achieving unit intensity) but then declines to a finite asymptotic value corresponding to that expected from the contribution of the (blue) wing of the probe laser, the fractional value of the spectral line intensity 40 cm^{-1} to the blue of the nominal wavelength, i.e., at λ_2^∞ for the free CN in the chosen state. Thus a pulsed laser wavelength scan, recorded at "long times" after the excitation pulse, portrays the effective absorption line shape of the free CN in the "detected" state. It is essentially an independent measurement of the laser pulse line shape: here it is found to be essentially Lorentzian with a half-width of $\gamma \cong 38$ cm^{-1}. Thus the expected transform-limited FWHM τ of the probe pulse would be expected to be ~ 185 fs. The experimental probe laser pulse width, convoluted with the pump width, was in this range,[2] consistent with this value. Thus, by "looking inward" from large t at different λ_2 values, we are mapping out the long-range potential $V_1(t)$ from such an $I(t,\lambda)$ surface.

FIG. 3. Simulated FTS data for the model system. The potential $V_1(t)$ is assumed be given by $V_1 = 300 \exp[-(t-200)/100]$ cm^{-1}, with t in fs. The probe-laser spectral profile is taken to be Lorentzian, with $\gamma = 40$ cm^{-1}. The upper potential $V_2(t)$ is assumed flat, as in Figs. 1 and 2. The left ordinate scale shows $V_1(t)$; the right one displays the calculated FTS transients for $\Delta = 0$, 40, and 80 cm^{-1} (calculated directly from the Lorentzian line shape, as described in the text). The zero of time here is arbitrary (Ref. 6).
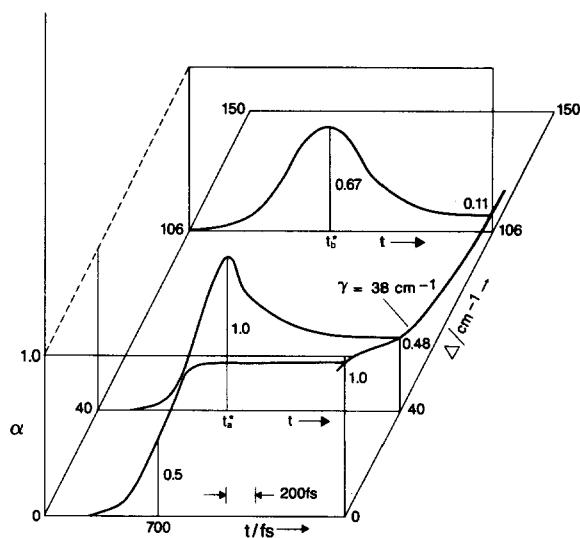

FIG. 4. Three-dimensional representation of $\alpha(t;\Delta)$ surface for FTS data of Ref. 2(a). The asymptotic signals are fitted by a Lorentzian with $\gamma \cong 38$ cm^{-1} as shown. The zero of time is arbitrary in this case.

Now let us be a little more quantitative. Suppose the spectral line shape of the probe is

$$g_\Delta(\delta) = g_\Delta(0)f(\delta), \tag{7}$$

where $g_\Delta(0)$ is the peak intensity at the nominal probe laser frequency for the given detuning Δ, and δ is the deviation (in wave numbers) from this nominal frequency. The line shape function is $f(\delta)$, with $0 \leqslant f(\delta) \leqslant f(0) = 1$. We note here that, for the special case of a Lorentzian line shape,

$$f_L(\delta) = \gamma^2/(\gamma^2 + \delta^2), \tag{8}$$

where γ is the half-width (in cm^{-1}), i.e., when $\pm \delta = \gamma$, $f(\delta) = \frac{1}{2}$.

The absorption (and thus the fluorescence intensity), say $I(t_i^*)$, of the separating fragment system at time t_i^* [corresponding to a potential $V_1(t_i^*)$] is proportional to the line shape function $f(\delta)$, where δ now represents the deviation D from the nominal probe frequency, i.e., $\delta \equiv D_\Delta$, when the probe laser has been set at a nominal detuning Δ. Thus,

$$I(t;\Delta) \equiv I(t_i^*) = I_{max} f(D_\Delta). \tag{9}$$

The deviance from the nominal probe frequency can be expressed in terms of the potential by

$$D_\Delta \equiv V_1(t_i^*) - \Delta, \tag{10}$$

with V_1 in cm^{-1} units. Note that D_Δ is implicitly a function of time through $V_1(t_i^*)$; i.e., $D_\Delta(t)$ evaluated at $t = t_i^*$.

Here, I_{max} is the maximum value of $I(t)$ that obtains when $D_\Delta = 0$ (and $f = 1$). For simplicity, we define a *relative* signal intensity $\alpha(t;\Delta) \equiv I(t;\Delta)/I_{max}$ and note that $\alpha(t;\Delta) = f(D_\Delta)$, where f is the line shape function of Eq. (7). (Recall that I_{max}, the peak intensity, should be independent of the probe laser detuning Δ.)

Let us consider the asymptotic conditions, for long times t, after $\alpha(t;\Delta)$ has become constant, i.e.,

$$\alpha(t;\Delta) \rightarrow \alpha(\infty;\Delta) \equiv \alpha_\infty(\Delta). \tag{11}$$

Measured values of $\alpha_\infty(\Delta)$ should reflect the absorption profile of the separated fragments, essentially the shape function $f(\Delta)$; i.e., we equate

$$\alpha_\infty(\Delta) = f(\Delta), \tag{12}$$

the laser wavelength profile. [From the experimental asymptotic values $\alpha_\infty(\Delta)$, one can then reconstruct $f(\Delta)$, i.e., the "effective" line shape function of the probe laser.]

We now recall from Eq. (9) that the temporal behavior of the detuned transient is given by that of D_Δ through $f(D_\Delta)$. Since $\alpha(t;\Delta) = f[D_\Delta(t)]$, we can evaluate $D_\Delta(t)$ directly from the experimental $\alpha(t;\Delta)$. We now outline the algorithm for the inversion product. First, construct the *inverse* function of $f(\delta)$, say $h(f)$. This will yield D_Δ as a function of $\alpha(t;\Delta)$. By definition of the inverse,

$$D_\Delta(t) = h[\alpha(t;\Delta)], \tag{13}$$

so that from Eq. (10),

$$V_1(t) - \Delta = h[\alpha(t;\Delta)]. \tag{14}$$

Thus the desired potential is given by

$$V_1(t) = \Delta + h(\alpha_t), \tag{15}$$

where we use the abbreviation $\alpha_t \equiv \alpha(t;\Delta)$. [Note that $h(\alpha_t)$ can be of positive or negative sign.] Equation (15) is

an explicit formula yielding the excited-state potential V_1 (in the region of large R; i.e., small detunings) directly from the $\alpha(t;\Delta)$ data base.

For the Lorentzian line shape case, using Eq. (8), Eq. (15) becomes

$$V_1(t) = \Delta \pm \gamma(\alpha_t^{-1} - 1)^{1/2}. \tag{16}$$

From Eq. (6), the $V_1(R)$ curve is immediately obtainable from the $V_1(t)$ points but with an abscissa defined only to within an unknown constant; i.e., the abscissa is a relative separation R or a "difference in R"; i.e., R + const.

We now illustrate the concept of the inversion procedure by a simple graphical example, shown in Fig. 5. As a data base, we employ the uncorrected "raw data"[6] FTS curves of Ref. 2; i.e., $I(t;\Delta)$ for $\Delta = 0, 40$, and $106 cm^{-1}$, and plot them as smoothed curves of $\alpha(t;\Delta)$. The asymptotic values $\alpha_\infty(\Delta)$ were fitted (see above) by a Lorentzian function [Eq. (8)] with $\gamma \simeq 38 cm^{-1}$; we take this as the line shape $f_L(\delta)$. First, we analyze the on-resonance transient ($\Delta = 0$) in Fig. 5(a). The smoothed α_t graph is aligned with the line shape function $f_L(\delta)$, where we identify the δ's with deviances D_Δ [Eq. (10)]; here, $D_0 = V_1(t_i^*)$. Taking a set of points α at convenient (e.g., equal) time intervals, we obtain a set of corresponding D_0 values ranging from essen-
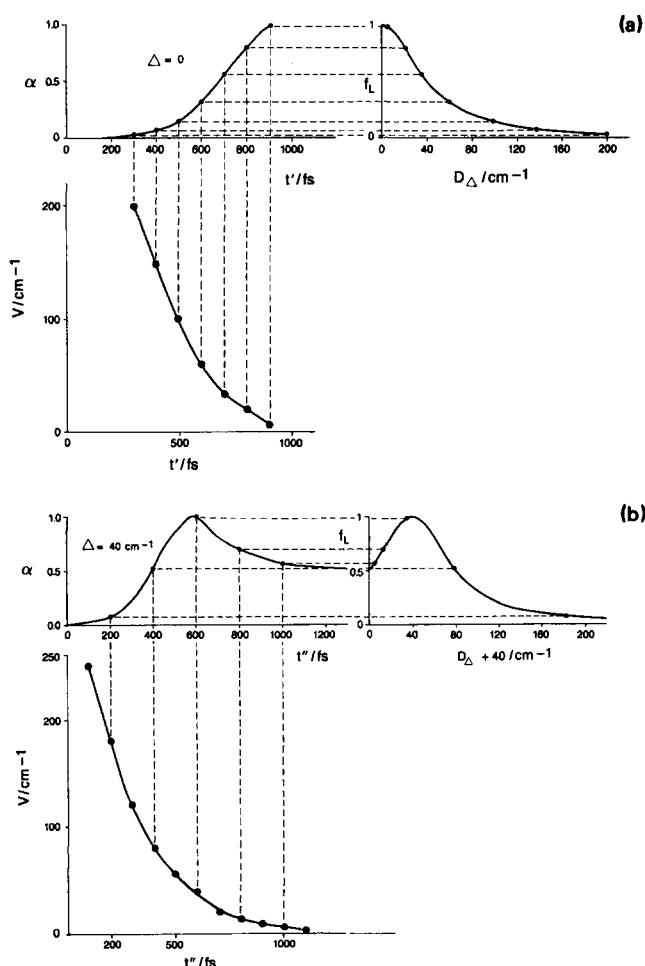

FIG. 5. Graphical analysis of FTS data of Ref. 2(a). (a) $\Delta = 0$, (b) $\Delta = 40$ cm^{-1}. Upper left: $\alpha(t)$; upper right: f_L; lower: derived $V_1(t)$ (see the text). The zero of time is arbitrary in this case.

tially zero to ~200 cm⁻¹, so that the results can be plotted in the form of $V_1(t_i^*)$ for each of the chosen t_i^*'s, shown below, defining a smooth curve of the desired potential $V_1(t)$ over the range 0–200 cm⁻¹. Next, we take the data set for $\Delta = 40$ cm⁻¹ [Fig. 5(b)]. Here, the line shape function $f(D_{\Delta=40})$ is plotted vs $D_\Delta + \Delta$; i.e., displaced by 40 cm⁻¹ such that the abscissa is V_1 [via Eq. (10)]. Once again, a set of points α is taken at convenient t_i^*; reading across to the f graph, we locate the values of $V_1(t_i^*)$, which are then plotted as $V_1(t)$, below. Note that here are two "branches" of the α_t graph corresponding to the two branches of the f graph; for $t<t_{max}$, α_t points correspond to positive values of D_Δ and for $t>t_{max}$, to negative D_Δ. Because of the detuning ($\Delta = 40$ cm⁻¹), this experiment probes V_1 up to a higher range of repulsions, roughly higher by the amount of the detuning, 40 cm⁻¹. Thus, the derived potential now extends to smaller t and larger V; the more so for larger detunings Δ (to the red). A composite $V_1(t)$ is shown in Fig. 6. It is clear that the spectral breadth of the probe laser is advantageous, in a limited way, because of the redundancy in the deduced $V_1(t)$ from the inversion procedure, which makes use of (at the very least) the entire FWHM in λ_2 to probe $V_1(t)$.

A somewhat more instructive illustration of the present inversion scheme is presented in what follows: a computer simula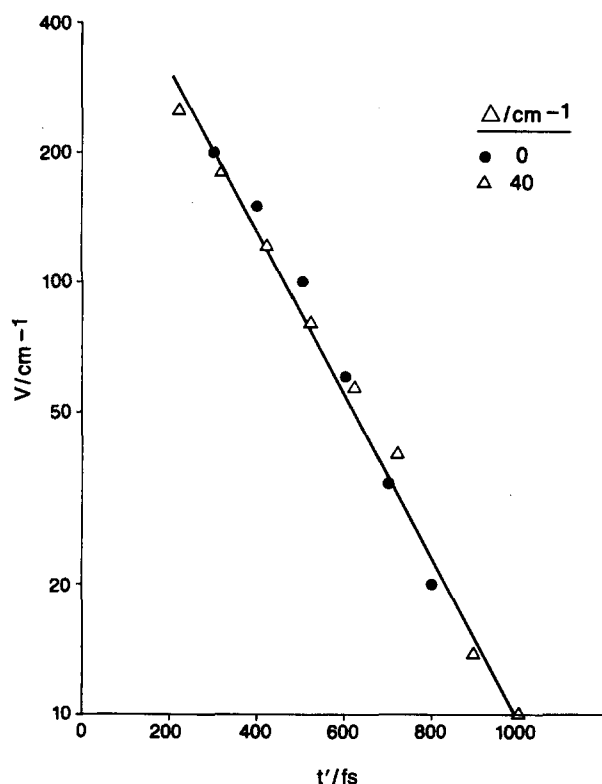tion of experimental "data" of the form of $I(t;\Delta)$, to which is added a random noise component to mimic typical experimental points. The resulting "data base" is inverted by an objective, bias-free computer algorithm to yield "experimentally derived" $V_1(t)$ points to compare with the originally assumed $V_1(t)$.

We take a simple analytical potential for $V_1(t)$, namely

$$V_1(t) = A \exp(-Bt) \qquad (17)$$

with constants chosen such that $V_1(t)$ is somewhat "realistic" (cf. Fig. 6). For simplicity, we assume a simple Lorentzian functional form for the spectral profile of the probe laser, Eq. (8), with $\gamma = 40$ cm⁻¹. Recall that,

$$\alpha(t;\Delta) = f[V(t) - \Delta]. \qquad (18)$$

For the Lorentzian profile, utilizing Eq. (8) for $f(\delta)$, we obtain

$$\alpha(t;\Delta) = \{1 + [(V-\Delta)/\gamma]^2\}^{-1}. \qquad (19)$$

Given the potential constants A and B, and the chosen γ, we

FIG. 6. Composite graph of $V(t)$ (semilog presentation), based on results of Fig. 5 for the FTS data for $\Delta = 0$ and 40 cm⁻¹. Because the time axes of the raw data curves were not related, a shift of 80 fs was arbitrarily applied to one of the $V(t)$ curves of Fig. 5 to bring both experiments into consistency. The resulting overall $V(t)$ graph shows the desired redundancy and extended range, up to about 300 cm⁻¹. The composite line drawn through the points is an exponential, $V = 300 \exp[-(t-200)/230]$ cm⁻¹, with t in fs (Ref. 6).

FIG. 7. Computer simulation of FTS data from an assumed $V_1(t)$, with computer inversion of each detunig "data set" to lead to the pointwise potential $V_1(t_i^*)$. (a) Solid curves: calculations [via Eq. (19)] of $\alpha(t;\Delta)$ for a model problem [flat V_2; exponential $V_1(t)$ from Eq. (17) with $A = 10^3$ cm⁻¹, $B = 10^{-2}$ (fs)⁻¹], at specified detunings Δ toward the red. Points: simulated experimental points obtained from smooth calculated curves by the addition of random noise with $\sigma = 0.02$. (b) Inversion of the simulation to yield $V_1(t)$ from Eq. (16). Symbols for points correspond to individual data points from panel (a). Solid curve: the input to the calculation, i.e., $V_1(t)$.

use Eq. (19) to compute the surface $\alpha(t;\Delta)$ in the form of curves of $\alpha(t)$, $0 < t \leqslant 750$ fs, for $\Delta = 0$, 25, 50, 100, and 150 cm^{-1}. To simulate data points, random noise increments $\delta\alpha$, chosen to yield a standard deviation $\sigma = 0.02$, are applied to $\alpha(t)$ at suitable values of t. Figure 7(a) displays the exactly calculated $\alpha(t)$ curves with typical set of simulated data points superimposed. It is these discrete data points are are now used in the inversion procedure.

From Eq. (19), we obtain experimental points $V_1(t_i)$ from

$$V_1(t_i) = \Delta \pm \gamma(\alpha_i^{-1} - 1)^{1/2} \qquad (16')$$

for each experimental data point α_i ($\equiv \alpha(t_i);\Delta$). Results are plotted in Fig. 7(b), showing the reduncancy associated with the overlapping data from differing detuning increments Δ. It is seen that the inverted $V_1(t_i)$ points are a satisfactory representation of the assumed $V_1(t)$, plotted as a smooth curve. The "noise" in the data is transmitted through the inversion procedure but is not significantly amplified in the resulted inverted potential; i.e., there is no deleterious "leverage" operating against the inversion. (This has been verified by a number of similar computer experiments with different level of random noise built into the data base.)

In all that has preceded, there has been an unrealistic assumption about the "flatness" of the second excited-state potential curve $V_2(t)$ in the long-range region; i.e., sufficiently large R such that R is linear in t [Eq. (6)]. Next, we consider the influence of a more realistic $V_2(t)$.

Case 2. Two repulsive surfaces

Figure 8 shows the simplest example of relevant potential curves, with both $V_1(t)$ and $V_2(t)$ being *monotonic, repulsive* functions. For the analysis that follows, we define a difference potential $\Delta V(t)$:

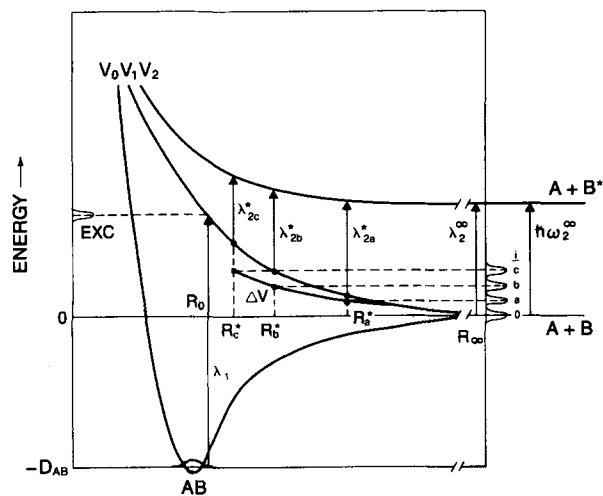$$\Delta V(t) = V_1(t) - V_2(t) + \hbar\omega_2^\infty, \qquad (20)$$

which governs the detuning; i.e., a given detuning increment Δ now corresponds to the difference potential $\Delta V(t)$ rather than to $V_1(t)$ as before [when $V_2(t) \cong \hbar\omega_2^\infty$ for time $t \geqslant t_{min}$]. Thus, the present inversion procedure now yields $\Delta V(t)$, rather than $V_1(t)$ itself. It is important to realize that the dynamics of the half-collision are governed entirely by E_{avl} and $V_1(t)$; it is only that the detection procedure (whether LIF or MPI) involves the energy difference $V_2(t) - V_1(t)$ and thus (at least in the simple example of Fig. 8) a given detuning Δ will now probe smaller values of t and thus larger values of $V_1(t)$. Note that, if $V_2(R)$ is "too similar" to $V_1(R)$, that at even small detunings Δ we are no longer probing in the long-range region of $V_1(R)$ and thus may have lost the linearity of R vs t and thereby the congruence between $V(R)$ and $V(t)$. However, if the smallest R probed, say $R*$, is such that $V_1[t(R*)] \ll E_{avl}$, then the inversion procedure will yield $\Delta V(t)$, where the conversion from $\Delta V(t)$ to $\Delta V(R)$ is governed only by the linearity R vs t of Eq. (6) with v calculated for the lower; i.e., the *dynamically relevant*, excited-state potential, $V_1(R)$. [Thus we employ the $R(t)$ relation for $V_1(R)$ to convert $\Delta V(t)$ to $\Delta V(R)$, regardless of the (irrelevant) possibility that $R(t)$ is nonlinear on $V_2(R)$ in the R range probed; only the trajectory on the lower curve $V_1(R)$ determines the lower limit of R for which the inversion procedure is valid.] As discussed later, when the pump pulse is tuned instead of the probe, information on $V_1(t)$ is obtained.

Case 3. Repulsion with an attractive van der Waals well

Next we consider the more realistic situation in which $V_1(R)$ [and possibly $V_2(R)$ as well] contains a long-range attractive (van der Waals) well. First let us examine the consequence of such a well in $V_1(R)$ [with a flat potential $V_2(R)$]; Fig. 9 shows an example. The main new feature is

FIG. 8. Schematic potentials for case 2: two repulsive potentials $V_1(R)$, $V_2(R)$ as shown; also $\Delta V_2(R)$ as defined by Eq. (20). V_0 and V_1 are the same as in Fig. 2. Vertical lines denote λ_{2a}^*, etc., indicate the probe-laser wavelengths required to excite the separating system at the specified separation R_a^*, etc. Because of the nonzero slope of V_2, the values of R_a^*, R_b^*, and R_c^*, etc., here are all smaller than those for the flat case V_2 (case 1) shown in Fig. 2. Here the probe "penetrates" to shorter separations and thus shorter separation times.

FIG. 9. Schematic potentials for case 3: $V_1(R)$ has a van der Waals well. Here we assume a flat $V_2(R)$, Vertical lines as before indicate the probe wavelengths for exciting the separating system at the specified separations. Note that the zero crossing of $V_1(R)$ leads to an on-resonance detection at a finite delay time at $R(0)$; for longer times, detection requires detuning to the *blue*. There is a maximum blue detuning corresponding to the van der Waals minimum, i.e., $-\Delta \leqslant \epsilon$ (see the text), here shown as $a'(\lambda_{2a'}^*)$. Detuning further to the blue results in the disappearance of any transient signal.

FIG. 10. Schematic potential $V_1(t)$ exhibiting a minimum, with $V_2(t)$ taken to be flat. Here we assume a constant spectral bandwidth $\delta\omega$ and a constant temporal bandwidth δt_L of the probe laser. The time interval required to traverse an energy range δV (shown equal to $\delta\omega = 2\gamma$) varies depending upon the slope of the potential. See the text for discussion of the consequences.

the transient crossing of the zero of the potential at a time t_0^*, so that, for on-resonance detection ($\Delta = 0$), a sharp rise in signal should occur but, instead of reaching consistancy, there is a peak only near t_0^*, followed by a decay. Here we also expect to be able to observe transient signals for *blue* shifts, provided that the magnitude of the detuning shift is less than the van der Waals well depth say ϵ:

$$-\Delta \leqslant \epsilon. \tag{21}$$

Tuning systematically to the blue, the disappearance of the transient signal should thus reveal the depth of the well in V_1.

Another feature of the expected transient behavior is illustrated in Fig. 10, namely, the trend in temporal response near the peak signals. As long as the time interval δt required to traverse a region of V_1 of δV governed by the probe laser spectral bandwith (e.g., $\delta V \cong 2\gamma$, as shown) is longer than the probe laser pulse duration δt_L, then the signal peak height should be constant, the same for all detunings Δ, namely, $\alpha_{peak} = \alpha_{max} = 1$. But for $\delta t < \delta t_L$, the peak intensity will be smaller:

$$\frac{\alpha_{peak}}{\alpha_{max}} = \alpha_{peak} \cong \frac{\delta t}{\delta t_L} < 1. \tag{22}$$

Here $\alpha_{peak} < 1$ because the time of passage of the recoiling fragments through the increment of time δt (and thus of separation δR) corresponding to δV is now shorter than the probe laser pulse duration, so the "duty factor" is less than unity. This fall-off of α_{peak} will *not* occur if $\delta t \geqslant \delta t_L$.

Let us now work out the dependence of this "critical" condition upon the potential. Since $\delta t = \delta V/\dot{V}_1$, where $\dot{V}_1 \equiv dV_1(R)/dt$,

$$(\dot{V}_1)_{crit} = \delta V/\delta t_L. \tag{23}$$

Thus, "too-fast passage" will occur if $\dot{V}_1 > (\dot{V}_1)_{crit} = \delta V/\delta t_L$. For the ideal case of a transform-limited pulse, $(hc\,\delta E)\delta t_L \simeq h$, so that for V in cm^{-1}, $\delta V = 1/c\delta t_L$. Thus, Eq. (23) for $(\dot{V}_1)_{crit}$ becomes

$$(\dot{V}_1)_{crit} = 1/c(\delta t_L)^2, \tag{24}$$

inversely proportional to the *square* of the pulse duration. [Thus, for $\delta t_L = 1$ ps, $(\dot{V}_1)_{crit} = 33$ cm^{-1} ps^{-1}; for $\delta t_L = 40$ fs, $(\dot{V}_1)_{crit} = 2.1 \times 10^4$ cm^{-1} ps^{-1} or a change of 840 cm^{-1} within one 40 fs pulse duration].

Making the connection to $V(R)$, we note that

$$\dot{V}_1 = \left(\frac{dV_1}{dR}\right)\dot{R} = F_1(R)\dot{R} \cong F_1(R)v, \tag{25}$$

where $F_1(R)$ is the magnitude of the force at R, and v is the terminal velocity [cf. Eq. (3)], since $\dot{R} \cong v$ in the long-range region of validity of Eq. (6). Thus,

$$(F_1)_{crit} = [cv(\delta t_L)^2]^{-1} \equiv F_{crit}. \tag{26}$$

Expressing the force in cm^{-1} Å^{-1}, v in km s^{-1} and δt_L in ps,

$$F_{crit}/cm^{-1} Å^{-1} = 3.3[(v/km\ s^{-1})(\delta t_L/ps)^2]^{-1}. \tag{27}$$

For $\delta t_L = 1$ ps and $v = 1$ km s^{-1}, $F_{crit} = 3.3$ cm^{-1} Å^{-1}, implying that the fast passage condition, $\alpha_{peak} \ll 1$, will apply except for very "flat" regions of the potential. For $\delta t_L = 40$ fs (keeping $v = 1$ km s^{-1}), $F_{crit} = 2 \times 10^3$ cm^{-1} Å^{-1}, a *much* less restrictive condition, so the "useful" range of R *, and thus of detunings Δ, over which $\alpha_{peak} = 1$ is much broader.

In summary, the problem of too-fast passage limits the observability of the detuned transients; the shorter the probe laser pulse duration, the larger the useful detuning range and thus the range of V_1 probed.

Case 4. Two potentials with attractive van der Waals wells

Finally, we consider the very general case in which both $V_1(R)$ *and* $V_2(R)$ posses long-range attractive wells. Several possibilities can be examined, as shown schematically in Figs. 11 and 12. Plotted in each panel are $V_1(t)$, $V_2(t)$ and the difference potential $\Delta V(t)$, defined in Eq. (20). The functional forms chosen were adaptations of Exp-6 potentials, but with t replacing R, i.e.,

$$V(t) = \epsilon[\exp(1 - Z) - 2Z^{-6}], \tag{28}$$

where ϵ is the well depth, $Z = t/t_m$ and t_m the time at which $V(t)$ is a minimum. The examples shown are for systems in which the upper and lower curves are displaced and of unequal well depths. In one case, $\Delta V(t)$ is positive at large t, implying red-shift detection, while for the other, $\Delta V(t)$ is negative at large t, passing through a minimum and becoming positive at smaller t (as in Fig. 10), thus indicating that blue-shift as well as red-shift detection will be successful. The existence of maxima and minima in $\Delta V(t)$ implies "rainbow-like" behavior, with double peaks and cutoff values of detunings Δ (either to the red or the blue).

Using the $\Delta V(t)$ from Fig. 11(a), calculating the t,λ spectra yields the detuned transients $\alpha(t;\Delta)$ shown in Fig. 11(b). After the introduction of noise as before ($\sigma = 0.02$), these "simulated experiments" have been inverted by the present method, characterized by Eq. (16). It is remarkable that the inversion leads to a recovery of the nonmonotonic $\Delta V(t)$ curves, as shown in Fig. 11(c). For the other case,

with a different shape of $\Delta V(t)$, analogous results are presented in Figs. 12(a), 12(b), and 12(c).

B. Shapes of transients and the asymptotes

In FTS experiments, the spectral width of the probe laser pulse is known at each value of the detuning Δ. In Fig. 13, a schematic illustration is presented that shows three spectral profiles (assumed to be Lorentzian, all of the same width

in frequency, namely, $\gamma = 50$ cm^{-1}), for the probe laser at $\Delta = 0$, 50, and 150 cm^{-1}, "looking in" at a potential that possesses a minimum.

For on-resonance detection, $\Delta = 0$, it is clear that there will be a peak, with $\alpha_{peak} = 1$, at $t(R_{\Delta_0})$, and, after a fall, another rise to a constant, asymptotic value of $\alpha = 1$. Note that, even for on-resonance detection ($\Delta = 0$) of the specified photofragment, the red wing of the probe laser profile
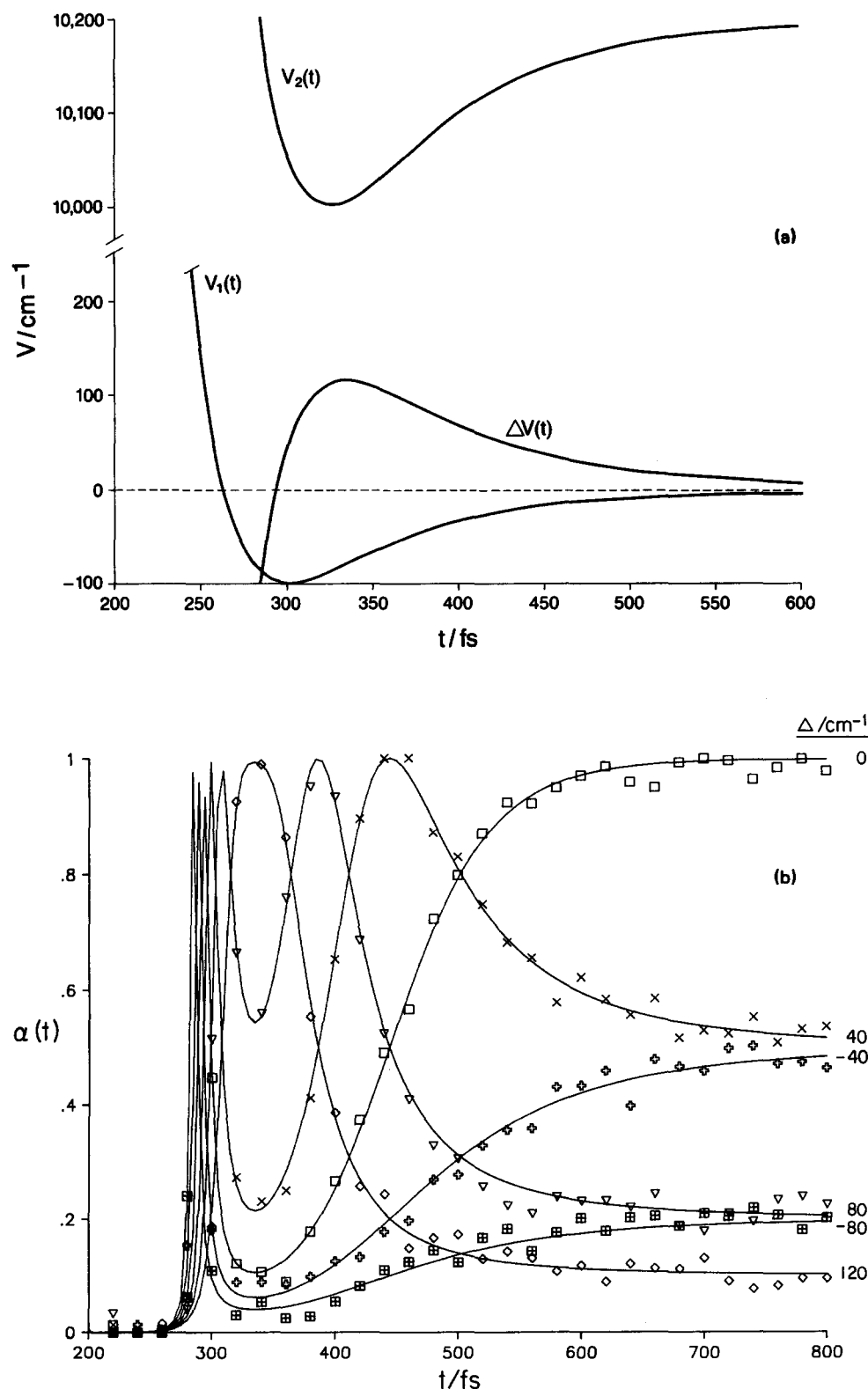
FIG. 11. Schematic potentials and FTS calculations for case 4: V_1 and V_2 with attractive van der Waals wells. (a) $V_1(t)$, $V_2(t)$, and $\Delta V(t)$, chosen so the difference potential is repulsive at long range (note that it possesses a maximum at shorter range, however). (b) Calculated transients, i.e., simulated FTS data similar to that of Fig. 7; solid curves are exact, points are calculated by the addition of random noise with $\sigma = 0.02$. (c) Inversion of the simulation to yield $\Delta V(t)$, via Eq. (16). As in Fig. 7, symbols for points correspond to individual data points from panel (b); solid curve is that from panel (a).
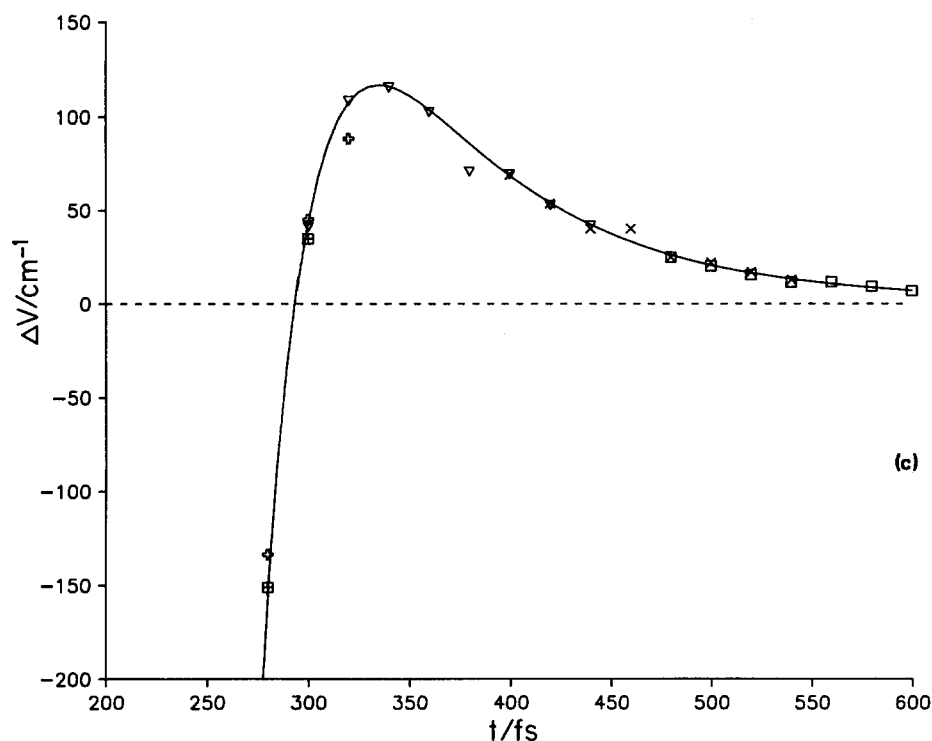
FIG. 11 *(continued)*.

will allow detection of the fragment at smaller separations R and thus earlier times t. For the examples shown, α would reach 1/10 at a time corresponding to R_{Δ_2} and 1/2 at a time $t^0_{1/2} \equiv t(R_{\Delta_1})$.

Now consider detuning by Δ_1 as shown (choosing $\Delta = \gamma$; i.e., 50 cm^{-1} to the red). Here, α will rise to its peak value, $\alpha_{peak} = 1$ (assuming the slow-passage limit) at a time corresponding to R_{Δ_1}; i.e., at $t(R_{\Delta_1}) \equiv t^0_{1/2}$ as defined above, based on the $\Delta = 0$ transient. Thereafter, α will decrease to

its asymptotic value, say $\alpha(\infty;\Delta_1)$ governed by the relative intensity of the blue wing of the probe laser, here 1/2 (since Δ_1 happens to be equal to the half-width γ of the frequency profile).

Next we predict the behavior for the larger detuning, $\Delta_2 = 3\gamma$. Here, α will rise to its peak value of unity at an earlier time, $t = t(R_{\Delta_2})$, which time also corresponds to the attainment of $\alpha = 1/10$ for the $\Delta = 0$ transient. Thereafter, α will decline to its asymptotic value $\alpha(\infty;\Delta_2)$, here 1/10
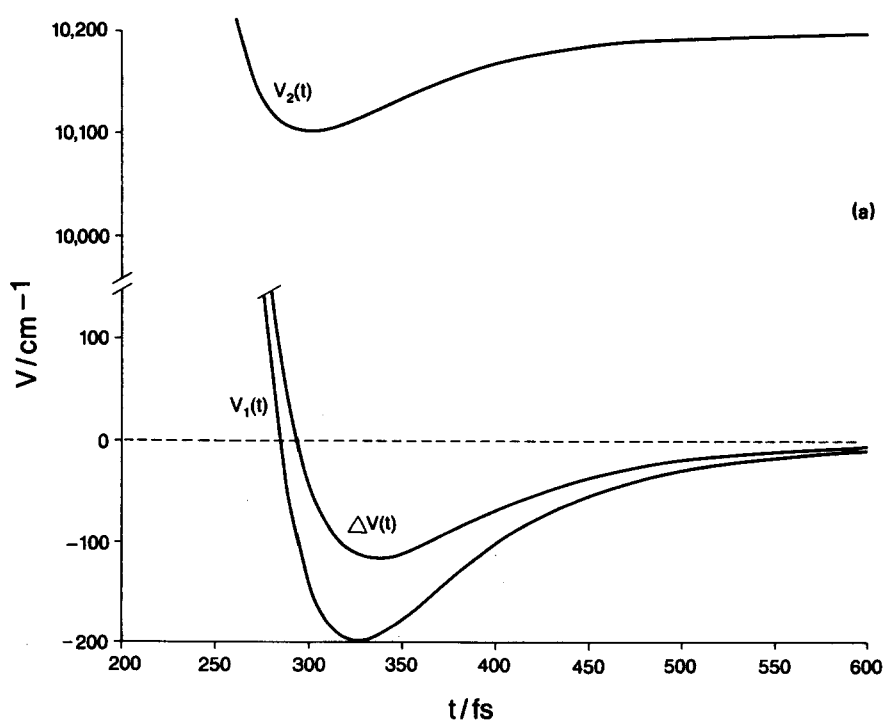
FIG. 12. Similar to Fig. 11, case 4, but with $V_1(t)$ and $V_2(t)$ chosen so $\Delta V(t)$ has a minmum at long range (panel a). (b) Calculated transients, as in Fig. 11; solid curves are exact, points are obtained by addition of noise with $\sigma = 0.02$. (c) Inversion of the simulation to yield $\Delta V(t)$ as in Fig. 11.
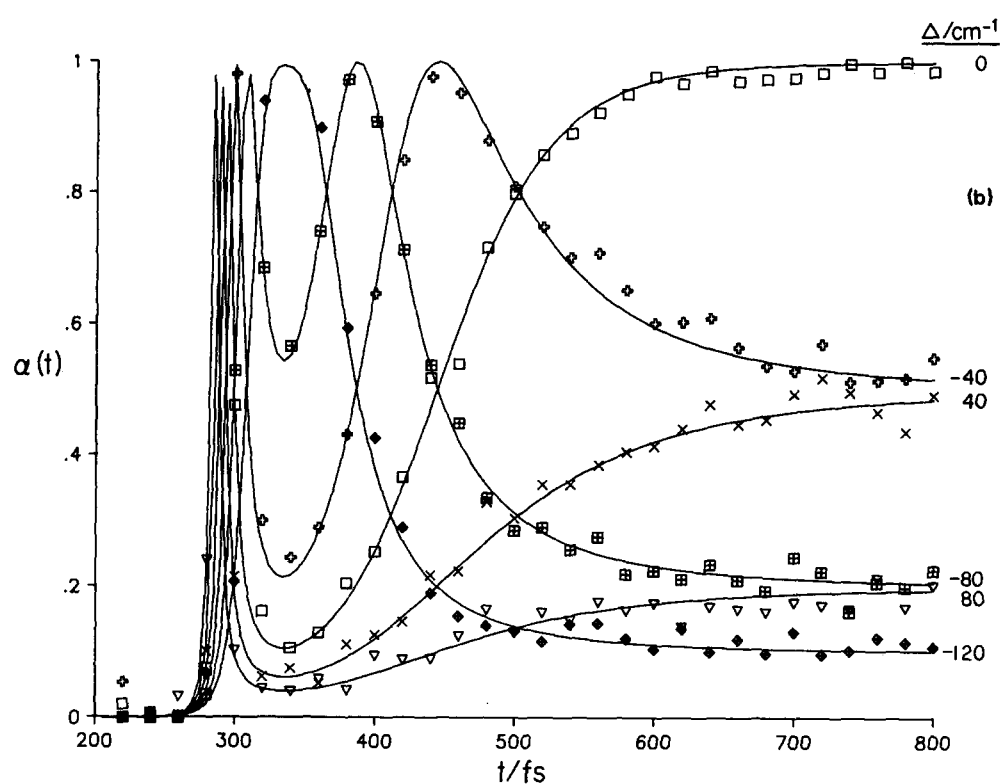
FIG. 12 (continued).
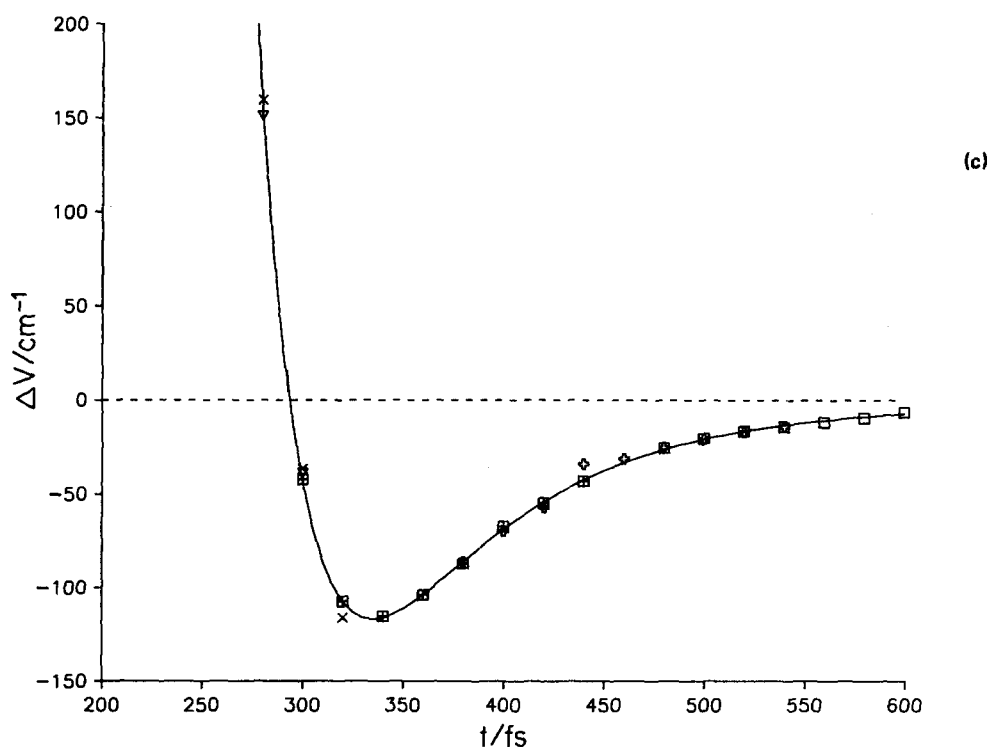
(based on the relative intensity of the blue wing of the probe laser detuned to Δ_2, as seen in Fig. 13).

Thus, the asymptotic signal levels $\alpha(\infty;\Delta_2)$ simply map out the spectral profile of the probe laser when tuned on resonance, i.e., $f(\delta)$ of Eq. (7), for $\Delta = 0$ (which is expected to be very similar in shape for all Δ's, as portrayed in Fig. 13). This is better illustrated in Fig. 4, based on the uncorrected experimental transients of Dantus et al.[2(a)] (As noted earlier, the asymptotic values of α are found to define a near-

Lorentzian function with a best-fit half-width $\gamma = 38 \pm 5$ cm^{-1}.)

The experimental implication of this subsection is that one can interpret the asymptotic signal levels $\alpha(\infty;\Delta)$ as the effective spectral line shape of the probe laser, i.e., $f(\delta)$ in Eq. (7), where δ is now identified with Δ above.

As seen in Fig. 13, if the potential V_2 (more correctly, the difference potential ΔV) has a minimum, probing with blue detuning out to the "rainbow edge" corresponding to
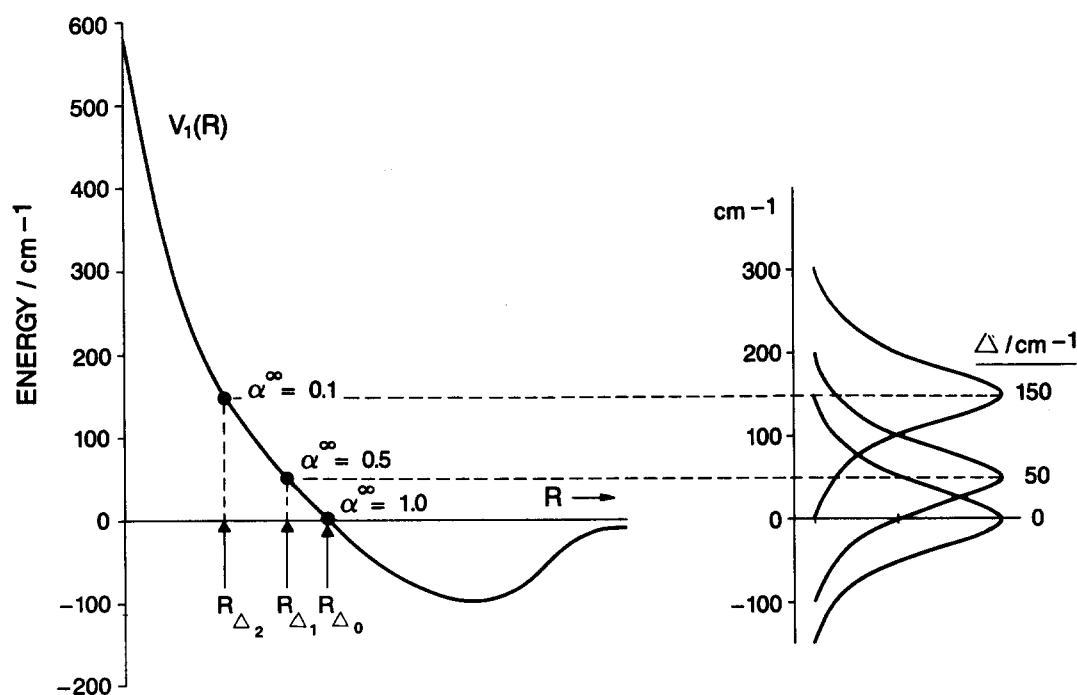
FIG. 13. Schematic potential $V_1(R)$ with van der Waals minimum [assuming flat $V_2(R)$]; probe laser spectral half-width taken to be $\gamma = 50$ cm^{-1}, detunings $\Delta = 0$, 50, and 100 cm^{-1}. For the on-resonance setting, i.e., $\Delta = 0$, the peak signal of the transient would occur at $t_0^*(R_{\Delta_0})$. However, at a shorter time, for the on-resonance transient, $t_1^*(R_{\Delta_1})$, where $V_1(R_{\Delta_1}) = \gamma$, the signal would reach $\alpha = 1/2$ (half-maximum); at still shorter time $t_2^*(R_{\Delta_2})$, where $V_1(R_{\Delta_2}) = 3\gamma$, the signal would reach 1/10 maximum, etc. Detuning by $\Delta = 50$ cm^{-1} would result in a transient peaking (with $\alpha = 1$) at $t_1^*(R_{\Delta_1})$, declining thereafter to an asymptotic value of $\alpha^\infty = 1/2$. Detuning by $\Delta = 150$ cm^{-1} would yield a transient peaking (with $\alpha = 1$) at $t_2^*(R_{\Delta_2})$, falling to an asymptotic value of $\alpha^\infty = 1/10$, etc. (see the text.)

the conditions of Eq. (21) should make it possible to evaluate the depth ϵ of the well in ΔV. From on resonance to this limit of the blue detuning, the asymptotic signals should be governed as above simply by the spectral line shape $f(\delta)$ of the probe laser.

C. Influence of pump laser wavelength

In Sec. II A, we have seen how it is possible to acquire information on the difference potential $\Delta V(t)$ by the inversion of the detuned transients. It would be desirable to "separate out" the upper (V_2) from the lower (V_1) potential, since it is the latter, i.e., the potential for the dissociating fragments, that is of fundamental interest for the purpose of femtochemical dynamics. After all, in the photoinitiated unimolecular reaction, the transition state is, by definition, located on $V_1(R)$ at separations $R \gg R_0$ (cf. Fig. 2). The role of V_2 is merely one of convenience for LIF detection (or, in a slightly different sense, for MPT detection). To gain information on $V_1(R)$, we can make use of on-resonance probe laser detection, but with systematic variation of the pump laser wavelength (i.e., variation of λ_1 at constant $\lambda_2 = \lambda_2^\infty$ in Fig. 2).

In what follows, we treat the simple example of this kind of pump-wavelength dependence study, and then consider some possible complications, which can limit the information obtainable from this pump-laser inversion scheme.

Case 1. Exponential repulsion

For simplicity, here we follow Bersohn and Zewail[5] and assume an exponential repulsive potential for V_1 and a flat potential for V_2. Thus,

$$V_1(R) = A \exp(-R/L), \tag{29a}$$

so

$$V_1(R_0) = E = A \exp(-R_0/L), \tag{29b}$$

i.e.,

$$V_1(R) = E \exp[-(R - R_0)/L]. \tag{29c}$$

From Fig. 2, it is recognized that E is simply E_{avl}, so Eq. (3) has been written as $\dot{R} = v(1 - V_1/E)^{1/2}$. We denote by $t_0^*(E,\Delta)$ the time required for the separation of the fragments from their initial value R_0 to that, $R^*(\Delta)$, interrogated by the probe laser at a chosen, constant value of the detuning Δ. This is the observable "delay time" from the pump pulse to the peak of the $\alpha(t;\Delta)$ signal. It can be evaluated via the quadrature:

$$t_0^*(E;\Delta) = \int_{R_0}^{R^*} \frac{dR}{\dot{R}} = \frac{1}{v} \int_{R_0}^{R^*} dR/(1 - V_1/E)^{1/2}, \tag{30}$$

where $v = (2E/\mu)^{1/2} \equiv v(E)$.

For the assumed potential of Eq. (29), this leads to

$$t_0^*(E;\Delta)v(E) = \int_0^{x^*} L\, dx/(1 - e^{-x})^{1/2}, \tag{31}$$

where $x \equiv (R - R_0)/L$ and $x^* = x(R^*)$. Thus, simplifying the notation in an obvious way, and evaluating the integral,

$$tv = Lx^* + 2L \ln[1 + (1 - e^{-x^*})^{1/2}]$$
$$\simeq (R^* - R_0) + 2L \ln 2 = c(\Delta) - R_0, \tag{32}$$

where $c(\Delta)$ is a constant at the given detuning Δ of the probe laser. However, both R_0 and v are functions of E.

Here, we have made the usual assumption, as in Sec. II A, that $E_{avl} \gg V_1(R^*)$ [cf. Eq. (4)]. The result (32) is

that the product tv depends linearly upon $R * - R_0$, as might have been expected.

We now express R_0 in terms of E by using Eq. (29b):

$$R_0 = L \ln(A/E),\tag{33}$$

so

$$tv \simeq R * - L \ln(A/4) + L \ln E,\tag{34}$$

or

$$t_0^*(E;\Delta)v(E) = L \ln E + a(\Delta),\tag{35}$$

where $a(\Delta) \equiv R *(\Delta) - L \ln(A/4)$ is another constant at the given detuning Δ, held fixed for the pump laser wavelength dependence study under consideration.

Thus, a plot of vt vs $\ln E$ should be nearly linear, with slope L, i.e.,

$$\frac{d(vt)}{d \ln E} \simeq L,\tag{36}$$

irrespective of Δ. (This result is implicit in the work of Bersohn and Zewail.[5])

We recall that, for the assumed exponential potential, $L = -d \ln V/dR$ and $R_0 = d \ln A/E$, so

$$L = -\frac{dR_0}{d \ln E} \simeq \frac{d(vt)}{d \ln E}\tag{37}$$

or

$$-\frac{dR_0}{dE} \simeq \frac{d(vt)}{dE}\tag{38}$$

consistent with Eq. (32). Thus, we learn about the energy dependence of R_0 [and thus the local slope $(dV/dR)_{R_0}$] from the observable dependence of vt upon E. Of course, for a very steep potential $[L \ll R_0(E)]$, vt will be essentially constant [cf. Eq. (36)] over a small range of E since, via Eqs. (32) or (39), tv is essentially measuring $R_0(E)$ on a 1:1 basis.

In conclusion, from the slope of a plot of vt vs $\ln E$ one obtains essentially the logarithmic derivative of the potential $V_1(R)$ in the neighborhood of $R_0(E)$. It can be conjectured that this result is nearly independent of the shape of the potential at larger separations; i.e., that small excursions in E yield "local" information about the potential near R_0, irrespective of the functional form of the potential. This will be examined in the next case considered.

Before leaving this subsection, we can make contact with an earlier general result [i.e., Eq. (6)]. Equation (34) can be rewritten:

$$R *(\Delta) \simeq v(E)t_0^*(E;\Delta) + F(E),\tag{39}$$

where $F(E)$ is an obvious function of E.

Thus, for a pair of experiments at fixed E,

$$R *(\Delta_2) - R *(\Delta_1) = v(E)\left[t_0^*(E;\Delta_2) - t_0^*(E;\Delta_1)\right]\tag{40a}$$

i.e.,

$$R_2^* - R_1^* = v(t_2^* - t_1^*)\tag{40b}$$

(in simplified notation), in accord with Eq. (6).

Case 2. Linearized potential

As an extreme case, we consider a linearized potential for V_1, obtained by expanding in x around R_0, namely

$$\frac{V_1(R)}{E} \simeq 1 - x + \frac{x^2}{2} + \cdots,\tag{41}$$

where, as before, $x \equiv (R - R_0)/L$, here assumed < 1. Retaining only the linear term (neglecting the higher-order terms in x), we have for the denominator of Eq. (30) simply x. Thus we obtain, by integration,

$$tv = 2L^{1/2}(R * - R_0)^{1/2},\tag{42}$$

where, as before, $R * = R *(\Delta)$.

This result differs in a fundamental way from that of Eq. (32), in which the product tv is linear in $R * - R$, as expected. The reason is apparently the too-early truncation of the expansion of the potential [Eq. (41)].

Case 3. Inverse-power repulsive potential

Here, we consider an inverse-power repulsive potential for $V_1(R)$ of the form

$$V_1/E = (R_0/R)^n.\tag{43}$$

Thus, from Eq. (30),

$$tv = \int_{R_0}^{R *} \frac{dR}{[1 - (R_0/R)^n]^{1/2}}.\tag{44}$$

Letting $y = R_0/R$ and $y^* = R_0/R *$, this becomes

$$tv = R_0 \int_1^{y^*} \frac{(-dy)}{y^2(1 - y^n)^{1/2}},\tag{45}$$

the only elementary solution of which is for $n = 2$. Here, we find

$$tv = R_0 \frac{(1 - y^{*2})^{1/2}}{y^*} = (R^{*2} - R_0^2)^{1/2}$$
$$= (R * - R_0)^{1/2}(R * + R_0)^{1/2},\tag{46}$$

where, as before, $R * = R *(\Delta)$.

As for case 2, the result is nonlinear in $R * - R_0$, so the simple and near-intuitive result found for the exponential repulsive potential (case 1) cannot be considered general. Nevertheless, for case 3 as for case 2, pump-laser wavelength variation experiments carried out at fixed probe-laser wavelength (and thus at constant $R *$) do appear to be sensitive to the energy dependence of R_0 and thus to the shape of the repulsive potential near the separation $R_0(E)$.

Such experiments should probably be analyzed according to case 1, i.e., by examining the pump-laser energy dependence of the vt product, which, to a zero-order approximation, should be constant. Deviations from constancy, if detected, should indeed lead to information on $V_1(R)$ near R_0.

III. INFLUENCE OF OTHER DEGREES OF FREEDOM: BEYOND THE SIMPLE DIATOMIC

Thus far, we have considered only the simplest situation, namely, the dissociation of a diatomic (or quasidiatomic) molecule proceeding via photoexcitation from an attractive ground electronic state to the repulsive branch of an accessible excited electronic state. For this case, the present inversion procedure should be appropriate to the extent that the motion of the separating atoms can be approximated by classical mechanics. The conditions for the validity of the

classical mechanical treatment of collisions and half-collisions are well known. Recent quantum mechanical (wave packet) simulation of the ICN experiments[7] has actually reproduced the main features of the classical mechanical model.[5]

There are several classes of diatomics that fail to satisfy the criterion of a single, simple repulsive state, e.g., cases involving excitation to predissociating states or states that involve curve crossing en route to dissociation. It goes without saying that, for triatomic (or polyatomic) molecules, the additional vibrational and rotational degrees of freedom will significantly complicate any simple, one-dimensional classical approach. In what follows, we shall consider briefly the influence of these complications with a view to preserving some of the advantages of the present, simple inversion technique.

A. Diatomics

Here we consider two (related) sources of complications to the present inversion treatment for diatomics. Case 1 concerns the role of a predissociating excited state and case 2, to a repulsive one that involves curve crossing in the exit channel.

Case 1: Predissociation and the interhalogens

There are many well-known examples of excited states of diatomics that are predissociative, i.e., whose potential curves $V(R)$ have a well, followed by a (rotationless) barrier en route to dissociation. This leads to the familiar "breaking off" of the emission spectrum at a definite value of the vibrational quantum number as well as the appearance of a few diffuse rotational lines in absorption associated with tunneling through the barrier (near its maximum) (Ref. 8). Well-studied examples include the $B(^3\Pi_{0+})$ states of the diatomic interhalogen molecules, e.g., IBr, ICl, and BrF (Ref. 9). The origin of the barrier is the "intersection" or avoided crossing at $R = R_x$ of two diabatic potential curves of the same symmetry leading to a pair of adiabatic curves, whose splitting is $\Delta E(R_x) = 2H_{12}(R_x)$, where H_{12} is the matrix element of the Hamiltonian coupling the two states. The barrier height is related simply to the energy at the crossing point by subtracting half the splitting; i.e., $H_{12}(R_x)$ (Ref. 10).

Oscillatory behavior in the predissociation behavior in the spectra of diatomics is also observed and interpreted in terms of resonances (quasibound states below the barrier and in the neighborhood of the barrier maximum) (Ref. 11). From the present viewpoint, provided that the barrier maximum is located at relatively small R and its height exceeds the greatest red detuning (Δ) value of the probe laser, it should be possible to carry out FTS experiments and execute the present scheme to yield information on the long-range part of the repulsive $B(^3\Pi_{0+})$ potential. This implies feasibility for the three above-mentioned interhalogens, whose barriers are all $> 550 \text{ cm}^{-1}$.

Case 2. Curve crossing and alkali halides

Of more immediate relevance is another class of diatomics, namely, the alkali halides (MX), two of which, NaI and

NaBr, have now been studied using the FTS method.[3] Here the femtosecond pump pulse excites the salt molecule to a repulsive, covalent state. As the MX falls apart, reaching internuclear distances close to the crossing point R_x between the covalent (M + X products) and ionic ($M^+ + X^-$ products) diabats, depending upon the relative velocity at R_x, there is a finite probability of continuing along the diabat to form M + X or being trapped within the adiabatic well.

The experimental results[3] show convincing evidence of "trapping resonances." A semiquantitative analysis confirms the interpretation, based on fairly well-known potentials and standard Landau–Zener curve-crossing theory. A simple wave-packet theory seems well suited for the description of the overall process,[12] and the present classical mechanical inversion procedure for these "curve-crossing systems" can easily be extended.

B. Triatomics

The first molecule to be studied experimentally using FTS was the triatomic ICN,[1,2] and the detuning experiments interpreted[2] using a quasidiatomic approximation (which treatment formed the basis for the present approach to the inversion problem). Obviously, the presence of a diatomic fragment, here CN, forces one to consider the additional degrees of freedom of CN.

First of all, even at the classical mechanical level, there are a variety of trajectories of the separating particles associated with the formation of the CN in different vibrational and rotational states (for the given electronic state). These originate from the different initial configurations and phases of the intramolecular motions of the triatomic.

There are classical models that contain the essential physics of the process.[13] They relate the initial bond angle of the electronically excited triatomic to an impact parameter b and to the final rotational angular momentum of the diatomic fragment, also taking into account the initial rotational angular momentum (if any) of the ground-state triatomic. For the simplest case of a linear excited state, and for a rotationally cold triatomic, there should be negligible rotational excitation in the product so the centrifugal potential will be small and the effective potential $[V_{1\text{eff}}(R,b) = V_1(R) + Eb^2/R^2]$ not very much different from $V_1(R)$, so the present analysis would still be appropriate.

Even for situations in which the diatomic is substantially rotationally excited, as long as a specific J state is being probed and thus a specified relative velocity v used in the analysis, the results may yield information on the effective potential $V_{1\text{eff}}(R)$ for a fairly well-defined b, from which $V_1(R)$ might be deduced. In other words, by careful analysis of the $I(t,\Delta)$ surface for different rotational states, one may be able to construct the angular dependence of the potential.[2(e)] A full classical trajectory (or better, quantal) simulation like those of Ref. 14, a posteriori, would be helpful to "close the loop" and confirm the potentials that establish the dynamics of the half-collision.

C. Symmetric tops and larger molecules

Photofragmentation dynamics of symmetric-top molecules, like the alkyl halides, have been studied by many

workers.[15] As early as 1937, Fink, Porret, and Goodeve[16] showed that the continuum absorption spectra of the methyl halides could be well explained by a simple quasidiatomic approximation involving repulsive excited-state "pseudo"-potentials $V_1(R)$ with R the separation between the center of mass of the methyl radical and the halogen atom. This model was extended to isotopic methyl halides[17] and checked for consistency by measurements of isotope effects in the photolysis of methyl bromide.[18] To the extent that the diatomic model is appropriate to describe the photofragmentation, the present inversion technique is applicable.

Recently, picosecond transient detuning experiments in molecular beams have been reported[4] for CH_3I and, although the transients were too fast to be resolved on the ps scale, both the red- and blue-shift asymptotic signal levels, $\alpha(\infty;\Delta)$, showed the expected behavior, i.e., mirroring the effective spectral line shape of the probe laser.

A more reasonable approximation for the methyl halides is the pseudotriatomic model used by Shapiro and Bersohn,[19] in which the three H atoms are assumed to remain in a plane and to vibrate with respect to the carbon (and thus to the halogen). The near-resonant Raman observations of Imre et al.[20] require a model of at least triatomic character where the dissociating coordinate and the umbrella motion are considered explicitly. FTS experiments on these systems should reveal the coupling among the different degrees of freedom in a manner similar to the studies made for alkali halide systems.[3]

IV. CONCLUDING REMARKS

In this paper, we have presented a method for inverting femtosecond transition-state spectral data to obtain the potential energy surface (curve) for the dissociating molecules, making use of the key FTS observables: the $I(t;\lambda)$ surface and the asymptotic wavelength dependence of the intensity of the transient signals. Illustrative inversion procedures have been demonstrated using the "raw" experimental FTS data[6] of Dantus et al.,[2(a)] on ICN and computer-simulated "experiments" for model systems. (Because the recoil velocity of fragments is typically of the order of 1 km s^{-1}, FTS experiments promise subangstrom "inversion resolution" on the PES.)

The analysis presented in this paper represents an entrée into the more general treatments of FTS data to deal with angular-dependent potentials and the PESs of larger systems.

The coherence of the system was considered only through the γ of the probe laser, but in the future it may be possible to separate the coherence of the laser and the dephasing of the transition at λ_2^∞ or $\lambda_2^\ddagger$, using well-known techniques such as correlation functions or density matrices.[21]

Our goal has been to develop and illustrate a pracitcal process of inversion and to discuss its possible applications to present and future experiments. The simple method of inversion presented here demonstrates that FTS is indeed a direct probe of the potential at different interfragment separations.

[1]N. F. Scherer, J. L. Knee, D. D. Smith, and A. H. Zewail, J. Phys. Chem. 89, 5141 (1985).
[2](a) M. Dantus, M. J. Rosker, and A. H. Zewail, J. Chem. Phys. 87, 2395 (1987); (b) M. J. Rosker, M. Dantus, and A. H. Zewail, Science 241, 200 (1988); (c) M. Dantus, M. J. Rosker, and A. H. Zewail, J. Chem. Phys. 89, 6113 (1988); (d) M. Dantus, M. J. Rosker, and A. H. Zewail, ibid. 89, 6128 (1988); (e) A. H. Zewail, Faraday Discuss. Chem. Soc. (in press).
[3](a) T. S. Rose, M. J. Rosker, and A. H. Zewail, J. Chem. Phys. 88, 6672 (1988); (b) M. J. Rosker, T. S. Rose, and A. H. Zewail, Chem. Phys. Lett. 146, 175 (1988).
[4](a) L. R. Khundkar and A. H. Zewail, Chem. Phys. Lett. 142, 426 (1987); (b) J. L. Knee and A. H. Zewail, Spectroscopy 3, 44 (1988), and references therein.
[5]R. Bersohn and A. H. Zewail, Ber. Bunsenges. Phys. Chem. 92, 373 (1988).
[6]The data of Ref. 2(a) have recently been analyzed in detail [Refs. 2(c) and 2(d)] to account for convolution effects and for the recent measurement of $t = 0$ [Ref. 2(b)]. Here, we consider the raw data only for the sake of illustration.
[7]S. O. Williams and D. G. Imre, J. Phys. Chem. (in press).
[8]G. Herzberg, Molecular Spectra and Molecular Structure. I. Spectra of Diatomic Molecules (Van Nostrand, New York, 1950), Chap. VII.
[9]M. S. Child and R. B. Bernstein, J. Chem. Phys. 59, 5916 (1973); see also M. B. Faist and R. B. Bernstein, ibid. 64, 2971 (1976); 68, 2022(E) (1978).
[10]R. B. Bernstein, Chemical Dynamics via Molecular Beam and Laser Techniques (Oxford, New York, 1982), Chap. 8.
[11]See, for example, (a) M. S. Child, in Atom–Molecule Collision Theory, edited by R. B. Bernstein (Plenum, New York, 1979), Chap. 13; (b) M. S. Child, in Specialist Periodical Reports, Vol. 2 (Chemical Society, London, 1974).
[12]V. Engel, H. Metiu, R. Almeida, R. A. Marcus, and A. H. Zewail, Chem. Phys. Lett. 152, 1 (1988).
[13]See, for example, J. P. Simons and P. W. Tasker, Mol. Phys. 27, 1691 (1974).
[14]See, for example, M. D. Pattengill, Chem. Phys. Lett. 78, 229 (1983); Chem. Phys. 87, 419 (1984), and R. Schinke, J. Phys. Chem. 93, 3195 (1988), and references therein.
[15]See, for example, Molecular Photodissociation Dynamics, edited by M. N. R. Ashford and J. E. Baggott (Royal Society of Chemistry, UK, 1987).
[16](a) CH_3Br: P. Fink and C. F. Goodeve, Proc. R. Soc. London Ser. A 163, 592 (1937); (b) CH_3I: D. Porret and C. F. Goodeve, ibid. 165, 31 (1938).
[17]A. A. Gordus and R. B. Bernstein, J. Chem. Phys. 22, 790 (1954).
[18]A. A. Gordus and R. B. Bernstein, J. Chem. Phys. 30, 973 (1959).
[19]M. Shapiro and R. Bersohn, J. Chem. Phys. 73, 3810 (1980); see also M. Shapiro, J. Phys. Chem. 90, 3644 (1986), and references therein.
[20]D. Imre, J. L. Kinsey, A. Sinha, and J. Krenos, J. Phys. Chem. 88, 3956 (1984); R. L. Sundberg, D. Imre, M. O. Hale, J. L. Kinsey, and R. D. Coalson, ibid. 90, 5001 (1986).
[21]See, for example, S. Mukamel, in Ultrafast Phenomena VI (Springer, New York, 1988).